Published in final edited form as:
*Nat Cell Biol*. 2013 December ; 15(12): 1495–1506. doi:10.1038/ncb2879.

# Senescent cells harbour features of the cancer epigenome

**Hazel A. Cruickshanks**[1,5,6], **Tony McBryan**[1,6], **David M. Nelson**[1], **Nathan D. VanderKraats**[2], **Parisha P. Shah**[3], **John van Tuyn**[1], **Taranjit Singh Rai**[1,5], **Claire Brock**[1], **Greg Donahue**[3], **Donncha S. Dunican**[4], **Mark E. Drotar**[1], **Richard R. Meehan**[4], **John R. Edwards**[2], **Shelley L. Berger**[3], and **Peter D. Adams**[1,7]

[1]Institute of Cancer Sciences, University of Glasgow and Beatson Institute for Cancer Research, Glasgow, G61 1BD, UK.

[2]Center for Pharmacogenomics, Washington University School of Medicine, St Louis, Missouri 63110, USA.

[3]Perelman School of Medicine, University of Pennsylvania, Philadelphia, Pennsylvania 19104, USA.

[4]MRC Human Genetics Unit at the Institute of Genetics and Molecular Medicine at the University of Edinburgh, Crewe Road, Edinburgh, EH4 2XU, UK.

## Abstract

Altered DNA methylation and associated destabilization of genome integrity and function is a hallmark of cancer. Replicative senescence is a tumour suppressor process that imposes a limit on the proliferative potential of normal cells that all cancer cells must bypass. Here we show by whole-genome single-nucleotide bisulfite sequencing that replicative senescent human cells exhibit widespread DNA hypomethylation and focal hypermethylation. Hypomethylation occurs preferentially at gene-poor, late-replicating, lamin-associated domains and is linked to mislocalization of the maintenance DNA methyltransferase (DNMT1) in cells approaching senescence. Low-level gains of methylation are enriched in CpG islands, including at genes whose methylation and silencing is thought to promote cancer. Gains and losses of methylation in replicative senescence are thus qualitatively similar to those in cancer, and this ‘reprogrammed’ methylation landscape is largely retained when cells bypass senescence. Consequently, the DNA

[7]Correspondence should be addressed to P.D.A. (p.adams@beatson.gla.ac.uk).
[5]Present addresses: MRC Human Genetics Unit at the Institute of Genetics and Molecular Medicine at the University of Edinburgh, Crewe Road, Edinburgh, EH4 2XU, UK; (H.A.C.); Institute of Biomedical and Environmental Health Research, University of the West of Scotland, Paisley, PA1 2BE, UK (T.S.R.).
[6]These authors contributed equally to this work.

Note: Supplementary Information is available in the online version of the paper

**AUTHOR CONTRIBUTIONS**

H.A.C. carried out the bulk of the experiments. D.M.N., P.P.S., J.v.T., T.S.R., C.B., M.E.D. and D.S.D. carried out further experiments. T.M. carried out the bulk of the data analysis. N.D.V. and G.D. carried out further data analyses. H.A.C. and T.M. provided substantial and critical intellectual input. R.R.M., J.R.E. and S.L.B. provided further intellectual input. P.D.A., H.A.C. and T.M. conceived the project and wrote the manuscript.

**COMPETING FINANCIAL INTERESTS**

The authors declare no competing financial interests.

**Accession numbers**. Primary accessions—Bisulfite sequencing of proliferating, senescent and SV40 bypass cells (GSE36640). Referenced accessions—Gene expression array (GSE36616)) and lamin B1 chromatin immunoprecipitation sequencing (GSE32399) in matched cells[18], bisulfite sequencing raw data (GSE29127; ref. 3), cDMRs (GSE32399; ref. 35).

methylome of senescent cells might promote malignancy, if these cells escape the proliferative barrier.

The DNA methylomes of cancer cells exhibit many aberrations when compared with normal cells. This includes DNA hypo- and hypermethylation and associated transcriptional de-repression, gene silencing and genome instability. Global DNA hypomethylation is thought to cause expression and recombination of repetitive sequences leading to instability of the cancer genome, whereas hypermethylation at CpG islands can contribute to cell transformation by silencing tumour suppressor genes[1,2]. More recent studies have also linked DNA hypomethylation in cancer cells to formation of repressive chromatin domains and gene silencing[3]. The origin of these aberrations is unknown, but may be linked to perturbations in the DNA modification machinery.

Cellular senescence is a stable proliferation arrest and an important tumour suppressor mechanism[4–7]. For example, replicative senescence blocks tumour formation by imposing an upper limit on the proliferative capacity of normal cells[8,9]. To become fully transformed, cancer cells must bypass senescence (by circumventing or inactivating the senescence barrier before or after its imposition, respectively). Chromatin changes are apparent in senescent cells, but they are only beginning to be characterized at the whole genome level[10–18]. There is no comprehensive analysis of DNA methylation in senescent cells. Therefore, we set out to comprehensively map and compare the DNA methylome of proliferating and replicatively senescent cells.

## RESULTS

### Global hypomethylation and focal hypermethylation in senescence

IMR90 cells undergo replicative senescence after prolonged passage in culture through a combination of shortened telomeres and induction of p16INK4a (p16; ref. 19). Senescent IMR90 cells exhibited characteristic features of senescence, including proliferation arrest, enlarged morphology, expression of senescence-associated β-galactosidase (SA β-gal) activity and p16, repression of cyclin A, and chromatin changes marked by senescence-associated heterochromatin foci (SAHFs) and recruitment of the histone chaperone, HIRA, to PML (promyelocytic leukemia) nuclear bodies (Supplementary Figs 1a–i)[4,12,19]. Moreover, gene expression profiling of these cells showed altered expression of many genes[18], including repression of proliferation-promoting genes (Supplementary Figs 2a–c), and upregulation of many inflammatory mediators comprising another hallmark of senescence, the senescence-associated secretory phenotype (Supplementary Fig. 21d)[20].

Initially, to compare DNA methylation in proliferating and senescent cells, we stained cells with an antibody to 5′-methylcytosine. Consistent with previous global analyses in cultured primary human cells[14], this showed a decrease in overall DNA methylation in senescent cells (Fig. 1a,b). Previous studies have indicated that the overall methylation level of immortal cells in culture is relatively stable[14,21], suggesting that the changes observed are not solely due to extended growth in culture, but are linked to a finite proliferative lifespan. To determine DNA methylation profiles across the whole genome, we carried out single-

nucleotide bisulfite sequencing (in excess of 15× coverage in triplicate) of proliferating and senescent cells, yielding a total of 314.7 Gbp) of sequence data (Supplementary Table 1). Analysis of the data confirmed an overall decrease in cytosine methylation in senescent cells (Fig. 1c), from 65.0 to 58.4% methylcytosine basecalls, out of all basecalls at reference CpG sites. Individual replicates of proliferating and senescent cells were highly concordant (Supplementary Tables 2 and 3 and Fig. 3a), with paired Pearson coefficients ranging from 0.88 to 0.92 between like samples (Supplementary Table 4). Absolute levels and changes in methylation at non-CpG sites, CHG and CHH (defined in Supplementary Methods), were negligible (proliferating to senescent, 0.44–0.41% (CHG) and 0.42–0.43% (CHH); Supplementary Tables 5 and 6), compared with the frequency of failed bisulfite conversion of unmethylated C to U (Supplementary Table 7). Net hypomethylation in senescence consisted of hypo- and hypermethylation events, although hypomethylation exceeded hypermethylation (Fig. 1d and Supplementary Table 8).

As reported previously[22], proliferating IMR90 cells contained interspersed regions of near-complete and partial methylation. When compared with proliferating cells, senescent cells showed extended regions of substantial hypomethylation, predominantly at regions of partial methylation in proliferating cells (Fig. 1e and Supplementary Fig. 3). In addition, senescent cells contained focal regions of hypermethylation (Fig. 1d–f and Supplementary Fig. 3b). We used a sliding and expanding window approach to identify contiguous significant (false discovery rate, FDR < 0.05) differentially methylated regions in senescence (sDMRs, defined in Supplementary Methods). There were more hypomethylated than hypermethylated sDMRs, and the former were several fold longer and of greater magnitude than the latter (Fig. 1g–j and Supplementary Fig. 3b).

As senescence involves many programmed changes in gene expression (Supplementary Fig. 2a–d; ref. 18), we asked whether alterations in methylation correlate with these changes. Senescence-associated hypomethylation at genes generally occurred at those genes expressed at low levels in proliferating cells (Supplementary Fig. 4a–c) and, typically, was not associated with changes in gene expression, regardless of whether it occurred at gene bodies or promoters (Supplementary Fig. 4d,e). As gene promoters containing CpG islands are typically hypomethylated, as expected we observed little further hypomethylation at these sites (Supplementary Fig. 4c,f).

When compared with hypomethylation, the magnitude of gene promoter and body hypermethylation in senescent cells was typically modest (Supplementary Fig. 4a,b,d,e). However, this was distributed more equally across low-, intermediate- and high-expression genes, with some bias towards low-expression genes (Supplementary Fig. 4a–c). Interestingly, compared with hypomethylation, hypermethylation was more likely to occur at genes whose expression increased or decreased in senescence (Supplementary Fig. 4d–e). Indeed, amongst expressed genes in proliferating cells, there was a significant ($P = 0.0014$) bias towards increased methylation of the promoter and downregulation in senescence (Fig. 2a and Supplementary Fig. 4g). The set of genes harbouring a CpG island, expressed in proliferating cells, and showing increased methylation in senescence included many cell cycle genes whose repression contributes to senescence-associated proliferation arrest, including histones (*HIST1H2BM* and *HIST1H2AE*), *CCNA2*, *CENPA*, *MCM2* and *TOP2A*

(Supplementary Table 9). Of the 221 genes in Supplementary Table 9, 122 decreased and eight increased their expression in senescence. By Ingenuity Pathway Analysis (IPA) the top ranked 'biofunction' of all 221 genes in this dataset is 'Cell Cycle' (Supplementary Table 10).

To extend this analysis, we adopted a more sophisticated approach for discovering differential methylation patterns associated with changes in gene expression. In this recently described approach[23], differential methylation was represented as an interpolated curve, or signature, and groups of genes with similarly shaped signatures and corresponding expression changes were identified (Fig. 2b,c). This approach identified a set of 139 genes (Supplementary Table 11). Of these, expression of 136 decreased in senescence, typically associated with increased DNA methylation at promoter proximal regions either side of the CpG island (Fig. 2d,e and Supplementary Fig. 5 and 11). IPA showed the top-ranked biofunction of this set to again be 'Cell Cycle' (Supplementary Table 12), and there was substantial and highly significant overlap of the genes in Supplementary Tables 9 and 11. Specifically, of 221 and 139 genes in Supplementary Tables 9 and 11 respectively, 49 were in common (27.0-fold enrichment over random, $P < 0.0001$; Fig. 2f). In sum, two independent analyses showed that increased promoter methylation, particularly flanking CpG islands, is associated with repression of cell cycle genes in senescence.

## Hypomethylation occurs at late-replicating lamin-associated domains (LADs)

Next, we wanted to understand the process of hypomethylation in senescence. First, we set out to determine whether hypomethylation occurs by a failure of maintenance methylation in proliferating cells or active demethylation in senescent cells. We observed that hypomethylation was already detectable in cyclin A-positive proliferating cells as the population approached replicative senescence (near-senescent; Fig. 3a). Moreover, we failed to detect ongoing loss of methylation in senescent cells after proliferation arrest (Fig. 3b). Together, these results suggest that hypomethylation occurs in cells approaching senescence (near-senescent cells) before proliferation arrest, suggesting a failure of maintenance methylation by the DNA methyltransferase, DNMT1 (ref. 24). As shown previously[25], expression of DNMT1 was repressed in senescent cells (Fig. 3c–e). More significantly, in cells approaching senescence, we observed subnuclear relocalization of DNMT1 (Fig. 3f,g). Specifically, in near-senescent cells there was a marked reduction in proliferating cyclin A-positive cells with nuclear DNMT1 puncta, compared with proliferating cells (Fig. 3f,g). Previous studies have shown that S-phase DNMT1 puncta are localized to late-replicating heterochromatic regions of the nucleus[24]. Indeed, we confirmed that some DNMT1 foci in proliferating cells co-localized with a constitutive heterochromatic sequence, such as pericentromeric satellite 2 (Fig. 3h). Unlike DNMT1, there was no change in the number of replication factories nor their assembly at satellite 2 sequences, as judged by PCNA foci (Fig. 3i–j). In line with altered DNMT1 localization, satellite 2 was hypomethylated in senescent cells as shown previously[26,27], and demonstrated by bisulfite sequencing and methylation-sensitive Southern blotting (Fig. 4a,b). Failure of these sequences to recruit DNMT1 was also accompanied by the de-compaction of their chromatin and upregulation of transcription, as shown here by fluorescence *in situ* hybridization (FISH) and reverse-transcription PCR (RT-PCR) respectively (see Fig. 4c–g) for a control genic sequence).

Moreover, knockdown of *DNMT1* triggered accelerated cellular senescence as shown previously[28,29], on the basis of proliferation arrest, repression of cyclin A and expression of SA β-gal (Supplementary Fig. 6a–d); and also expression of satellite 2 and other chromatin changes characteristic of senescence (specifically, appearance of SAHFs and recruitment of histone chaperone HIRA to PML nuclear bodies[11,12]; Supplementary Fig. 6e–g). A previous report showed that late-replicating sequences are progressively demethylated over cumulative cell divisions[30]. Our results show that, in near-senescent cells, DNMT1 fails to localize normally to late-replicating satellite 2 sequences, and this is associated with their DNA hypomethylation.

To test whether DNA hypomethylation was globally enriched at late-replicating sequences, we compared regions of hypomethylation in senescent fibroblasts with early- and late-replicating sequences in fibroblasts, using a data set generated previously[31]. This confirmed enrichment of hypomethylation at late-replicating sequences (Fig. 5a,b and Supplementary Table 13). Conversely, there was depletion of hypomethylation from early-replicating sequences (Fig. 5a,e and Supplementary Table 13). Whereas hypermethylated regions covered only a small proportion of the genome (7.3% in hypermethylated sDMRs), resulting in small absolute overlap with much larger early- and late-replicating regions, hypermethylation was significantly enriched in early-replicating regions and depleted from late-replicating regions (Fig. 5a,c,d and Supplementary Table 13). Previous studies have shown co-localization of DNA replication sites in late S-phase with LADs and nuclear lamin B1 foci[32–34]. Indeed, there was enrichment of hypomethylation at LADs (ref. 18), but a significant depletion of hypermethylation (Fig. 5a,f,g and Supplementary Table 13). Early-replicating DNA sequences tend to be gene rich[31], and approximately 60% of gene promoters contain CpG islands. Accordingly, there was an obvious enrichment of hypermethylation and depletion of hypomethylation at these sites (Fig. 5a,h,i and Supplementary Table 13). Together, these results indicate that hypermethylation is found preferentially at CpG islands. In contrast, hypomethylation in senescence occurs preferentially at gene-poor, late-replicating LADs and is linked to mislocalization of DNMT1 in near-senescent cells.

## Methylation changes in senescence resemble those in cancer

The widespread hypomethylation at late-replicating regions and LADs, as well as focal hypermethylation at CpG islands, are reminiscent of methylation changes previously reported in cancer[1,3,35,36]. In addition, aberrant transcription of satellite 2 has been noted in many cancer cells[37]. Therefore, we directly addressed whether the gains and losses of DNA methylation observed in senescence overlap with those in cancer. Specifically, we compared sDMRs in IMR90 cells with cancer DMRs (cDMRs) reported previously for colon and breast cancer[3,35,36]. Remarkably, when scored across the whole genome, we observed partial but highly significant overlaps between altered methylation events in cancer and senescence. Hypermethylated sDMRs were enriched at hypermethylated cDMRs (Fig. 6a,b and Supplementary Tables 14, 15, 16). Similarly, hypomethylated sDMRs were enriched at hypomethylated cDMRs, this being particularly marked for larger DMRs (Fig. 6a,c and Supplementary Fig. 6h and Supplementary Tables 14, 15, 16). Conversely, hypermethylated sDMRs were depleted from hypomethylated cDMRs (Fig. 6a,d and Supplementary Tables

14, 15, 16), and hypomethylated sDMRs were depleted from hypermethylated cDMRs (Fig. 6a,e and Supplementary Tables 14, 15, 16). More specifically, several CpG islands whose hypermethylation was previously reported to predict a cancer CpG island methylator phenotype showed small increases in methylation in senescence (namely, *RUNX3*, *CACNA1G*, *SFRP2*, *SOCS1* and *NEUROG1*; refs 38,39; Fig. 6f and Supplementary Fig. 7 and Supplementary Table 17). Interestingly, the promoter of *CDKN2A* (p19) did not show increased methylation within the CpG island itself, but a marked increase in the flanking regions either side (Supplementary Fig. 7). CpG island 'shores', close to designated islands, are themselves often targets of increased methylation in cancer[40]. In addition, we noted increased methylation within the CpG islands of two genes, *ESX1* and *IRAK3* (ref. 41), whose expression is incompatible with cancer cell survival (Supplementary Fig. 7 and Table 17).

Replicative senescence is a barrier to cell transformation[8,9]. In the process of malignant transformation, immortal cancer cells must evade replicative senescence. Our results suggest that features of the cancer methylome can be present in premalignant senescent cells, and perhaps propagated into cancer cells on escape from senescence. To test this, IMR90 cells approaching senescence were infected with a lentivirus encoding simian virus 40 (SV40) large T antigen to inactivate pRB and p53 and promote bypass of senescence (Fig. 7a,b), generating proliferating senescence 'bypass' cells (Supplementary Fig. 8a–c). Whole-genome bisulfite sequencing was carried out on bypass cells. The profile of DNA methylation in senescent cells was largely retained in bypass cells (Fig. 7c, top three tracks). Consequently, the difference between bypass and proliferating cells resembled the difference between senescent and proliferating cells, and the differences between bypass and senescent cells were less marked (Fig. 7c). Underscoring this, there was strong overall concordance between methylation in senescent cells and in bypass cells (Pearson $r = 0.955$), but poorer concordance between proliferating cells and bypass cells (Pearson $r = 0.900$; Fig. 7d). When DMRs were defined relative to proliferating cells, hypomethylated sDMRs significantly overlapped with hypomethylated bypass DMRs, and the same was true for hypermethylated DMRs (Supplementary Table 18). For example, 88.7% of hypomethylated sDMRs (>500 kb) are also observed in bypass cells (predicted random overlap = 26.4%) (Supplementary Table 18). Importantly, methylation changes retained in bypass cells were enriched for methylation changes in cancer (Supplementary Tables 19–21). For example, 88.4% of hypomethylated sDMRs that are retained in bypass cells are also observed in colon cancer cells (predicted random overlap = 39.6%; Supplementary Table 19, row 19). Specific CpG islands known to be methylated in cancer and shown here to acquire DNA methylation in senescence (CpG island methylator phenotype genes, *ESX1*, *IRAK3*), typically retained significant elevation of methylation in bypass cells (Supplementary Table 17). These data indicate that altered methylation acquired in senescent cells can be retained when these cells bypass senescence.

## DISCUSSION

Here we have shown that senescent cells harbour extensive changes to DNA methylation, compared with proliferating cells. First, senescent cells exhibit widespread hypomethylation in late-replicating, gene-poor regions, including pericentromeric satellites and LADs. As

normal cells approach their proliferative limit, altered regulation of DNMT1 is linked to DNA hypomethylation of these regions, and associated expression of satellite 2 repeats. Several recent studies underscore LADs as central to changes in nuclear and chromatin structure in senescent cells[17,18,42]. Whereas knockdown of *DNMT1* triggered premature senescence, we failed to observe delayed senescence on its ectopic expression. Conceivably, DNA hypomethylation of late-replicating regions is a sufficient trigger or effector of senescence, but is also redundant with other independent senescence triggers and effectors[4]. Suppression of DNMT1 may also trigger senescence by activation of DNA damage signalling[43]. Second, in senescent cells, a subset of repressed cell cycle genes exhibits increased DNA methylation at promoter-proximal regions either side of the CpG island. At these genes, DNA methylation might contribute to repression and so senescence-associated cell cycle exit and stable proliferation arrest[40]. Finally, increased methylation in senescent cells occurs disproportionately within CpG islands, regions that are typically free of DNA methylation. The physiological function of this low-level methylation is unclear, especially at genes whose CpG island methylation is thought to contribute to cancer, such as *SFRP2* and *IRAK3* (refs 41,44); in fact, here methylation may reflect a form of ‘epigenetic damage’ in stressed senescent cells (see below). Increases in DNA methylation might involve DNMTs other than DNMT1, such as the *de novo* methyltransferase DNMT3B (refs 25,45,46; Fig. 3c).

Our data support the view that altered methylation in cancer does not necessarily result from genetic alterations. Instead, features of the cancer methylome can originate in premalignant senescent cells, and be propagated into cancer cells on bypass of senescence. As cells progress to malignant cancer, acquired genetic changes and clonal selection will further mould the epigenome, probably leading to some differences between the epigenomes of senescent cells reported here and cancer cells[35]. Cancer cells might also acquire methylation changes independent of any altered methylation associated with senescence.

Both global hypomethylation and CpG island hypermethylation are thought to promote cancer[1,2,37,47,48]. Remarkably, some of the methylation changes observed in senescence are similar to those reported in cancer. In senescent cells, the extent of CpG island hypermethylation of CpG island methylator phenotype genes (and other genes silenced in cancer, such as *ESX1* and *IRAK3*) is small and probably not sufficient for transcription repression. However, we have also shown here that that altered methylation acquired in senescent cells can be retained in cells that bypass senescence. In such cells, and in the appropriate genetic context and tissue environment, low-level methylation in and around CpG islands of tumour suppressor genes, such as *CDKN2A* (p14), *IRAK3* and *SFRP2*, might be a seed to promote further hypermethylation and perhaps silencing[49–51]. Consistent with this idea, upregulation of DNMT3B is also associated with methylation of CpG islands in early stages of human colon cancer (for example hyperplastic polyps and adenomas)[52,53]. In a mouse model of mutant *BRAF*-induced colon cancer, upregulation of DNMT3B is associated with onset of cell senescence, and ultimately methylation of the CpG island of *CDKN2A* (p16), downregulation of p16 expression, bypass of senescence, and progression to cancer[54]. As hypomethylation is also a driver of genome instability and cancer[47,48], senescent cells that evade proliferation arrest might already harbour an unstable genome.

Moreover, hypomethylation is expected to facilitate expression and transposition of retrotransposons that further destabilize the cancer genome[55–57]. Indeed, increased transcription of retroelements in senescent human cells has been reported[58]. In sum, whereas senescence is a *bona fide* tumour suppression mechanism[4–9], if senescent cells can escape their proliferative barrier, they already harbour an epigenetic landscape likely to promote malignancy. As senescent cells accumulate within aged tissues[59–61], the altered epigenome of senescent cells might facilitate late-life onset of many human cancers[62] (Fig. 8).

## METHODS

Source data for several analyses are provided in Supplementary Table 22.

### Cell culture

IMR90 cells (Coriell) were grown in DMEM, high glucose (Life Technologies) supplemented with 20% fetal bovine serum, 2 mM L-glutamine and 100 μgml$^{-1}$ penicillin-streptomycin and incubated at 37°C with 20% (v/v) or 3% (v/v) $O_2$ and 5% (v/v) $CO_2$. Bisulfite sequencing was carried out on cells grown in 3% (v/v) $O_2$. Global DNA hypomethylation was also observed in 20% (v/v) $O_2$ (for example Figs 1a and 4b), and other experiments were carried out on cells grown under these conditions. Proliferating cells were PD 20–28 in 3% (v/v) or 20% (v/v) $O_2$, near-senescent cells were PD 54 in 20% (v/v) $O_2$ and senescent cells were PD 59 in 20% (v/v) $O_2$ and PD 88 in 3% (v/v) $O_2$.

### Antibodies and short hairpin RNAs (shRNAs)

See Supplementary Table 23.

### Generation and production of lentiviruses

For bypass of senescence, a SIN human immunodeficiency virus I (lenti-) vector expressing the early region of SV40 from the cytomegalovirus promoter and the gene encoding neomycin resistance, driven by the SV40 early promoter, was generated. Production of lentivectors and infection of IMR90 were carried out as described[65]. Infected cells were cultured in the presence of 500 μg ml$^{-1}$ G418 sulfate (Invitrogen) for one week.

### Immunofluorescence

Immunofluorescence was carried out broadly as described previously[12]. For staining with anti-5-methylcytosine, cells were fixed in paraformaldehyde and permeabilized with 0.2% (v/v) Triton X-100 in PBS (pH 7.5) for 2 min at room temperature, then incubated in 2 N HCl for 45 min at 37 °C to denature DNA. DNA was counterstained with an antibody to ssDNA in place of DAPI. Staining intensities were quantified using MetaMorph software (Molecular Devices).

### Senescence-associated β-galactosidase staining

Carried out as described in ref. 66.

### RT-PCR

Total RNA was extracted from cells using TRIzol (Life Technologies) according to the manufacturer's instructions. Before reverse transcription, total RNA samples were DNase I treated as recommended by the manufacturer (Life Technologies). Reverse-transcription reactions were carried out using SuperScript III (Life Technologies) following the manufacturer's protocol, using 1 μg of DNase I-treated total RNA as template. 1 μl of first-strand complementary DNA was used as a template for PCR. PCR conditions were as follows: 1 × PCR buffer, 0.2 mM deoxynucleotide triphosphates (Life Technologies), 0.25 μM forward primer, 0.25 μM reverse primer and 1.25 U *Taq* polymerase (Life Technologies). PCR reactions were incubated at 95 °C for 5 min followed by 30 cycles of 95 °C for 30 s, appropriate annealing temperature (primer pair dependent) for 30 s and 72 °C for 30 s, with a final incubation at 72 °C for 10 min. PCR products were analysed on an agarose gel. For quantitative RT-PCR, reverse-transcription reactions were set up as described above; 2 μl of reaction was used as a template for real-time PCR using inventoried TaqMan probes (Applied Biosystems) according to the manufacturer's instructions using a Chromo 4 real-time PCR machine (Bio-Rad).

### Gene expression array

RNA samples prepared as above were hybridized to a Human Genome U133 Plus 2.0 array (Affymetrix) according to the manufacturer's recommendations and as reported previously[18].

### RNA-seq

RNA-seq was carried out on an Illumina GAIIx instrument, according to the manufacturer's instructions. Full results of RNA-seq will be reported elsewhere.

### FISH

Cells grown on coverslips were hypotonically treated in 75 mM KCl for 20 min. Cells were fixed by adding drops of methanol:acetic acid (3:1), and finally incubated overnight in methanol:acetic acid (3:1) at −20 °C. The next day, coverslips were removed from fixative, steam dried and incubated in 100 μg $ml^{-1}$ RNase A in 2× saline-sodium citrate (SSC; pH 7.0) for 1h at 37 °C. Following washes in 2 × SSC, cover slips were incubated for 6 min at 37°C in 0.1 mg $ml^{-1}$ pepsin in acidic conditions. Following pepsin treatment, cells were post-fixed in 1% (w/v) parafomaldehyde. Subsequently, cells were dehydrated by successive incubations in 70%, 80% and 100% ethanol and dried. Once dried they were denatured by incubation in 70% (v/v) formamide and 2 × SSC at 73 °C for 5 min, dehydrated and dried as previously. Probes for FISH were prepared for hybridization according to the manufacturers' recommendations (Vysis and Exiqon), denatured at 73 °C for 5 min and pre-annealed for 1 h at 37°C. Probes were applied to coverslips and incubated at 37 ° C overnight. The following day coverslips were washed twice in 50% (v/v) formamide in 2 × SSC for 10 min at 43 °C, washed twice in 2 xSSC at 37 °C for 4 min, washed with 2 × SSC with DAPI for 4 min at room temperature and finally washed with 4 × SSC with 0.05% (v/v) Tween-20 for 5 min at room temperature. Slides were mounted with Prolong Gold (Life Technologies) and sealed. For co-FISH with an immunofluorescent stain for protein of

interest, cells were fixed as above and antibody staining was carried out as described. Following antibody staining, cells were post-fixed and treated as above with the omission of pepsin treatment. Areas of FISH probe signal were quantified using MetaMorph software (Molecular Devices).

### Western blotting

Carried out as described[67]. Uncropped western blots are shown in Supplementary Fig. 8d–e.

### Methylation-sensitive Southern blotting

1 μ*g* of genomic DNA was digested using the BstBI methyl-sensitive endonuclease. Fragments were separated by agarose gel electrophoresis and DNA was transferred onto a nylon membrane (Bio-Rad) by upward capillary motion in 0.4 M NaOH. DNA was immobilized on the membrane by baking at 80 °C. Blots were hybridized with a $^{32}$P-radiolabelled probe specific to the sequence of interest in hybridization solution (3 × SSC, 10 mM EDTA, 0.2% (w/v) polyvinylpyrrolidone, 0.2% (w/v) Ficoll, 0.2% (w/v) BSA, 0.1% (w/v) SDS, 0.04 mg ml$^{-1}$ salmon sperm DNA and 0.02 mg ml$^{-1}$ heparin, 9% (w/v) dextran sulfate). The following day, blots were washed in 2 × SSC/0.1% (w/v) SDS twice for 5 min at room temperature and twice in 0.1 × SSC/0.1% (w/v) SDS for 15 min at 65 °C. Membranes were exposed to autoradiograph film (Kodak) for imaging.

### Lamin B1 chromatin immunoprecipitation sequencing

Carried out as previously described[18].

### Bisulfite sequencing

500 ng of genomic DNA was bisulfite treated using an EZ DNA Methylation Gold kit following the manufacturer's recommendations (Zymo Research). Following treatment, PCR was carried out using conditions as above. Products were then directly cloned into pCR2.1 TA cloning vector following the manufacturer's protocol (Life Technologies) and those positive for inserts were sequenced.

### Whole-genome bisulfite sequencing

Carried out by BGI, Shenzhen.

### Representative experiments

All data shown as representative experiments, for example western blots and immunofluorescence, were repeated as shown at least three times.

### Data analysis/statistics

**Processing and alignment of bisulfite sequencing reads—**Sequence reads are transformed *in silico* to fully bisulfite-converted forward (C→T) and reverse (G → A) reads. The converted sequences are aligned against a converted human reference genome (hg18) in each combination: (1) forward (C → T) reads aligned to forward (C → T) genome; (2) reverse (G → A) reads aligned to reverse (G → A) genome; (3) forward (C → T) reads aligned to reverse (G → A) genome; (4) reverse (G → A) reads aligned to forward (C → T)

genome. During the library preparation process[68], genomic fragments representing alignments (3) and (4) are generated in the PCR step; however, they are not sequenced and only fragments corresponding to alignments (1) and (2) are read. As a result, only uniquely matching alignments from (1) and (2) are retained. Alignment was carried out using Bismark[69] (version 0.5.1), based on the Bowtie[68] aligner (version 0.12.7). Unaligned reads resulting from the initial alignments from these libraries were trimmed 15 bp from the 5′ end to remove the adapter sequences, as some libraries contained these sequences and realigned.

For each aligned sequence tag, the original unconverted sequence is compared against the original unconverted reference genome and the methylation status is inferred. Sequences aligned from (1) and (2) give information on cytosines on the forward and reverse strands respectively.

To remove PCR bias, a deduplication step removes potential duplicate reads, where both ends of the fragment align to the same genomic positions on the same strand, only one of the reads is retained. To control for potential incomplete bisulfite treatment any reads with more than three methylated cytosines in non-CpG contexts are discarded. Supplementary Table 1 details the sequence yields at each stage of this process. Supplementary Tables 2, 5 and 6 detail the number of methylated and un-methylated bases sequenced within CpG, CHG and CHH contexts (H = A, C or T).

Furthermore, reads are mapped against the unmethylated lambda genome, which was added to bisulfite sequencing reactions, giving the number of methylated bases, enabling the combined error rate resulting from sequencing errors and incomplete bisulfite conversion (Supplementary Table 7) to be determined.

**Identification of methylated cytosines—**Processed reads are aggregated on a per CpG basis (number of bases read supporting methylated/unmethylated status). At each reference cytosine the binomial distribution was used to identify whether a subset of the genomes within the sample were methylated at this location. Methylcytosines were identified while keeping the number of false positives below 1%. The probability of sequencing an observed number of cytosines given the identified error rates from the lambda alignment was determined using the binomial distribution. At each reference cytosine the number of trials in the binomial test was the read depth and the number of successes in the test was equal to the number of cytosines sequenced at that base. The probability was then corrected using the Benjamini–Hochberg (BH-) FDR function and the list of CpG sites was thresholded at the 0.01 FDR level. See Supplementary Table 3.

A two-tailed Fisher exact test was used to identify CpGs that were differentially methylated. Only CpGs determined using the binomial distribution in at least one sample, with at least three reads in at least one condition and with at least one read in the other condition, were considered for testing. *P*-values were corrected using the BH-FDR function to control false positives at a rate of 5%. See Supplementary Table 8.

**Identification of DMRs—**DMRs were calculated using a sliding window approach, window size 2kb. Windows start at an individual CpG and would extend 2kb, ending at the

final CpG contained within the window. At each window a two-tailed *G*-test of independence was carried out on both pooled and individual replicates. Total *G*-value was defined as the sum of the *G*-value for the individual replicates. Owing to the additive nature of *G*-tests, we were also able to compute a heterogeneous *G*-value (the difference between the total and pooled *G*-values). Each *G*-value was converted to a *P*-value using a chi-square distribution at high precision and the Python arbitrary precision mathematics (mpmath) package; this *P*-value represents the overall significance of the window taking into account the three replicates, whereas the *P*-value calculated from the heterogeneous *G*-value is to identify regions where replicates are significantly different.

*P*-values from pooled and heterogeneous *G*-tests were corrected using the BH-FDR function and transformed for display on the UCSC Genome Browser as $-10 \log_{10}(\text{FDR})$. Transformed *P*-values were multiplied by −1 if the pooled percentage methylation was lower in senescent samples than in proliferating samples (reflecting that hypomethylation is shown as a negative value). Difference *P* is a two-tailed *G*-test of independence on pooled samples for 2kb windows.

Windows within 4kb which had FDR corrected *P*-values of less than 0.05 were merged for both pooled and heterogeneous *P*-values and resulting regions smaller than 5kb were discarded. When comparing proliferating and senescent samples, 46 regions (spanning 353,622 bp—approximately 0.01% of the genome) were identified under these criteria as having significant FDR-adjusted *P*-values for heterogeneity, and these regions were removed from the proliferating versus senescence pooled DMR regions.

**Methylation difference plots—**Data bins were created for the integer values 0–100 and initialized as empty lists. For each CpG site within the pooled data, the methylation percentages for proliferating and senescent samples was calculated, considering only CpGs with minimum coverage of 10 reads in at least one sample and three reads in both samples. The methylation percentage of the proliferating sample was truncated to an integer value and used to select an appropriate data bin, into which the senescent sample methylation percentage was appended, and the average of each bin was computed, giving the corresponding final methylation percentage in senescent cells. Methylation difference was defined as the difference between starting and final average methylation percentages.

**Smoothed methylation plots—**The pooled whole-genome methylation data were processed using the BSmooth algorithm from the bsseq (v0.8.0) package within Bioconductor as described in refs 36,70. A modified version of the bsseq plotSmoothData function was created to plot the smoothed data with individual CpGs shown (addPoints = True) but suppressing the vertical ablines.

**Methylation versus expression plots—**Affymetrix raw data files (CEL) for each GeneChip were imported into R and analysed using the Bioconductor (http://www.bioconductor.org) packages. The GC Robust Multi-array Average method was used to background correct and normalize all samples. Each probe was mapped to an Ensembl gene identifier using the array's NetAffx annotation (version 29), and the fold change and expression in proliferating were mapped to the Ensembl gene identifier. Probes that mapped

to multiple distinct Ensembl genes were discarded. Where multiple probes map to a single gene the geometric average of the expression/fold change was calculated. Results were then plotted using the ggplot2 package within R.

**Correlation between replicates—**Replicates were compared pairwise, and for each CpG the methylation percentage for each replicate was calculated, for those CpGs with minimum coverages of 10 in one replicate and three in both replicates. The Pearson correlation coefficient was then calculated and results are presented in Supplementary Table 4.

**Determination of overlaps—**Overlaps were computed on a per base pair basis between two datasets (A and B). For every region within A the number of base pairs that were occupied by a region within B was computed. A permutation test was carried out to determine the background genomic average expected overlap. 1000 sets of regions with properties (length distribution and chromosome distribution) equal to those of set B were generated. Randomly generated regions of B were prevented from being generated within unsequenced regions of the genome (as defined by UCSC mapping and sequencing track—gap). The overlap of A and B was repeated for each randomly generated set of B to determine the average expected random overlap. *P*-values were estimated empirically from the observed overlaps of the randomly generated sets.

**Identification of altered methylation associated with altered gene expression —**This was carried out as described in ref. 23. For this approach, methylation signatures were created for each gene by interpolating the differential methylation scores over a fixed window relative to the gene's TSS. A curve similarity metric, the discrete Fréchet distance, was used to cluster genes together on the basis of the shape of the differential methylation data in the window. We then identified clusters of genes with similar patterns that have coordinated differential expression. To generate a gene list, we executed this procedure over many 5 kb windows around the TSS and selectively combined the results.

All three replicate pairs were pooled and cross-referenced with Ensembl to determine the TSS. Genes containing no sites with a differential methylation level of at least 0.2 within the window were removed. Genes for which methylation could not be interpolated owing to a low number of sites in the region were removed. Signatures were clustered for 23 5 kb windows overlapping every 500 bp, covering the area from 8 kb upstream of the TSS to 8 kb downstream. Clusters that were significantly up- or downregulated when compared with the overall set of expression values were then identified (Kolmogorov-Smirnov test; FDR < 0.05 using BH). The Fréchet distance was computed using a scaling factor between the *x* axis (bp) and *y* axis (differential methylation score) of 2,500 bp to one unit. A minimum cluster size of 10 and a minimum cluster purity of 0.85 were used. Gaussian smoothing ($\sigma = 30$) was applied to the signatures before clustering. A gene was included in the final list if at least two of its replicates were present in a significant cluster for at least two of the 5 kb windows.

One primary way in which false positives could be introduced with this method is for a cluster of genes to form at random whose expression values happen to be statistically

significant. As a control, we clustered the methylation curves and then scrambled their expression values before determining significant clusters and making a gene list as above. For 1,000 sets of scrambled expression values, we erroneously returned, on average, less than one gene per experiment (0.178). Of all experiments, 5.4% had one erroneous gene, 3.3% had two erroneous genes and 1.6% had three or more erroneous genes.

For the metagene analysis in Fig. 2 and Supplementary Table 11, the average differential methylation score was computed across all replicates and all genes downregulated in the final gene list.

### External data

**Late/early-replicating domains—**We determined domains of replication timing as in ref. 35 on the basis of the data from ref. 31. Percentage normalized replication timing data were obtained (personal communication, Scott Hansen), and then we identified regions with a late:early $\log_2$-ratio (with a pseudocount of 1 added to both numerator and denominator of the ratio) of greater than or equal to 1.5 for late-replicating regions and less than or equal to −1.5 for early-replicating regions. Matching positions within 2kb were merged and regions larger than 100 kb were selected as late/early-replicating domains (yielding 1,029 late-replicating regions and 1,075 early-replicating domains).

**cDMRs—**Colon cancer DMRs were obtained from ref. 36 and converted to hg18 using the UCSC liftOver tool for direct comparison with our data. This resulted in a total of 13,455 hypo- and 2,865 hypermethylated cDMRs. A total of 73 regions failed to completely map to the hg18 assembly, whereas 18 mapped to unfinished or unassembled regions of the genome (that is chr6_random) and were discarded. Colon cancer DMRs were also obtained from ref. 35 (GSE48580). Briefly, domains identified in cancer cells as hyper/hypomethylated were downloaded (in hg18 format) and regions of hyper/hypomethylation in normal cells were subtracted using subtractBed (bedtools) with a minimum overlap of 50%. Breast cancer bisulfite sequencing raw data were obtained from ref. 3 (GSE29127) and were processed as above to generate DMRs.

## Supplementary Material

Refer to Web version on PubMed Central for supplementary material.

## Acknowledgments

Thanks to S. Pepper in the CRUK microarray facility and to S. Hansen for assistance with DNA replication timing data. Thanks to Beijing Genome Institute for bisulfite sequencing. Work in the laboratory of P.D.A. was funded by NIA Program Project P01 AG031862 and CRUK Program A10250. S.L.B.'s laboratory was funded by NIA Program Project P01 AG031862. R.R.M.'s laboratory was funded by the MRC and the BBSRC. P.D.A. thanks P. Cairns for critical formative discussions.

## References

1. Ting AH, McGarvey KM, Baylin SB. The cancer epigenome-components and functional correlates. Genes Dev. 2006; 20:3215–3231. [PubMed: 17158741]
2. Sproul D, Meehan RR. Genomic insights into cancer-associated aberrant CpG island hypermethylation. Brief Funct. Genomic. 2013; 12:174–190.

3. Hon GC, et al. Global DNA hypomethylation coupled to repressive chromatin domain formation and gene silencing in breast cancer. Genome. Res. 2012; 22:246–258. [PubMed: 22156296]
4. Kuilman T, Michaloglou C, Mooi WJ, Peeper DS. The essence of senescence. Genes Dev. 2010; 24:2463–2479. [PubMed: 21078816]
5. Michaloglou C, et al. BRAFE600-associated senescence-like cell cycle arrest of human naevi. Nature. 2005; 436:720–724. [PubMed: 16079850]
6. Chen Z, et al. Crucial role of p53-dependent cellular senescence in suppression of Pten-deficient tumorigenesis. Nature. 2005; 436:725–730. [PubMed: 16079851]
7. Braig M, et al. Oncogene-induced senescence as an initial barrier in lymphoma development. Nature. 2005; 436:660–665. [PubMed: 16079837]
8. Feldser DM, Greider CW. Short telomeres limit tumour progression *in vivo* by inducing senescence. Cancer Cell. 2007; 11:461–469. [PubMed: 17433785]
9. Cosme-Blanco W, et al. Telomere dysfunction suppresses spontaneous tumorigenesis *in vivo* by initiating p53-dependent cellular senescence. EMBO Rep. 2007; 8:497–503. [PubMed: 17396137]
10. Choi MR, et al. Genome-scale DNA methylation pattern profiling of human bone marrow mesenchymal stem cells in long-term culture. Exp. Mol. Med. 2012; 44:503–512. [PubMed: 22684242]
11. Narita, Metal. Rb-mediated heterochromatin formation and silencing of E2F target genes during cellular senescence. Cell. 2003; 113:703–716. [PubMed: 12809602]
12. Zhang R, et al. Formation of MacroH2A–containing senescence-associated heterochromatin foci and senescence driven by ASF1a and HIRA. Dev. Cell. 2005; 8:19–30. [PubMed: 15621527]
13. O'Sullivan RJ, Kubicek S, Schreiber SL, Karlseder J. Reduced histone biosynthesis and chromatin changes arising from a damage signal at telomeres. Nat. Struct. Mol. Biol. 2010; 17:1218–1225. [PubMed: 20890289]
14. Wilson VL, Jones PA. DNA methylation decreases in ageing but not in immortal cells. Science. 1983; 220:1055–1057. [PubMed: 6844925]
15. Schellenberg A, et al. Replicative senescence of mesenchymal stem cells causes DNA-methylation changes which correlate with repressive histone marks. Aging. 2011; 3:873–888. [PubMed: 22025769]
16. Chandra T, et al. Independence of repressive histone marks and chromatin compaction during senescent heterochromatic layer formation. Mol. Cell. 2012; 47:203–214. [PubMed: 22795131]
17. Sadaie M, et al. Redistribution of the Lamin B1 genomic binding profile affects rearrangement of heterochromatic domains and SAHF formation during senescence. Genes Dev. 2013; 27:1800–1808. [PubMed: 23964094]
18. Shah PP, et al. Lamin B1 depletion in senescent cells triggers large-scale changes in gene expression and the chromatin landscape. Genes Dev. 2013; 27:1787–1799. [PubMed: 23934658]
19. Forsyth NR, Evans AP, Shay JW, Wright WE. Developmental differences in the immortalization of lung fibroblasts by telomerase. Aging Cell. 2003; 2:235–243. [PubMed: 14570231]
20. Coppe JP, Desprez PY, Krtolica A, Campisi J. The senescence-associated secretory phenotype: the dark side of tumour suppression. Annu. Rev. Pathol. 2010; 5:99–118. [PubMed: 20078217]
21. Young JI, Sedivy JM, Smith JR. Telomerase expression in normal human fibroblasts stabilizes DNA 5-methylcytosine transferase I. J. Biol. Chem. 2003; 278:19904–19908. [PubMed: 12665523]
22. Lister R, et al. Human DNA methylomes at base resolution show widespread epigenomic differences. Nature. 2009; 462:315–322. [PubMed: 19829295]
23. Vanderkraats ND, Hiken JF, Decker KF, Edwards JR. Discovering high-resolution patterns of differential DNA methylation that correlate with gene expression changes. Nucleic Acids Res. 2013; 41:6816–6827. [PubMed: 23748561]
24. Leonhardt H, Page AW, Weier HU, Bestor TH. A targeting sequence directs DNA methyltransferase to sites of DNA replication in mammalian nuclei. Cell. 1992; 71:865–873. [PubMed: 1423634]

25. Lopatina N, et al. Differential maintenance and de novo methylating activity by three DNA methyltransferases in ageing and immortalized fibroblasts. J. Cell Biochem. 2002; 84:324–334. [PubMed: 11787061]
26. Suzuki T, Fujii M, Ayusawa D. Demethylation of classical satellite 2 and 3 DNA with chromosomal instability in senescent human fibroblasts. Exp. Gerontol. 2002; 37:1005–1014. [PubMed: 12213551]
27. Enukashvily NI, Donev R, Waisertreiger IS, Podgornaya OI. Human chromosome 1 satellite 3 DNA is decondensed, demethylated and transcribed in senescent cells and in A431 epithelial carcinoma cells. Cytogenet. Genome. Res. 2007; 118:42–54. [PubMed: 17901699]
28. Yamakoshi K, et al. Real-time *in vivo* imaging of p16Ink4a reveals cross talk with p53. J. Cell Biol. 2009; 186:393–407. [PubMed: 19667129]
29. Young JI, Smith JR. DNA methyltransferase inhibition in normal human fibroblasts induces a p21-dependent cell cycle withdrawal. J. Biol. Chem. 2001; 276:19610–19616. [PubMed: 11259405]
30. Aran D, Toperoff G, Rosenberg M, Hellman A. Replication timing-related and gene body-specific methylation of active human genes. Hum. Mol. Genet. 2011; 20:670–680. [PubMed: 21112978]
31. Hansen RS, et al. Sequencing newly replicated DNA reveals widespread plasticity in human replication timing. Proc. Natl Acad. Sci. USA. 2010; 107:139–144. [PubMed: 19966280]
32. Moir RD, Montag-Lowy M, Goldman RD. Dynamic properties of nuclear lamins: lamin B is associated with sites of DNA replication. J. Cell Biol. 1994; 125:1201–1212. [PubMed: 7911470]
33. Peric-Hupkes D, et al. Molecular maps of the reorganization of genome-nuclear lamina interactions during differentiation. Mol. Cell. 2010; 38:603–613. [PubMed: 20513434]
34. Yaffe E, et al. Comparative analysis of DNA replication timing reveals conserved large-scale chromosomal architecture. PLoS Genet. 2010; 6:e1001011. [PubMed: 20617169]
35. Berman BP, et al. Regions of focal DNA hypermethylation and long-range hypomethylation in colorectal cancer coincide with nuclear lamina-associated domains. Nat. Genet. 2012; 44:40–46. [PubMed: 22120008]
36. Hansen KD, et al. Increased methylation variation in epigenetic domains across cancer types. Nat. Genet. 2011; 43:768–775. [PubMed: 21706001]
37. Ting DT, et al. Aberrant overexpression of satellite repeats in pancreatic and other epithelial cancers. Science. 2011; 331:593–596. [PubMed: 21233348]
38. Toyota M, et al. CpG island methylator phenotype in colorectal cancer. Proc. Natl Acad. Sci. USA. 1999; 96:8681–8686. [PubMed: 10411935]
39. Weisenberger DJ, et al. CpG island methylator phenotype underlies sporadic microsatellite instability and is tightly associated with BRAF mutation in colorectal cancer. Nat. Genet. 2006; 38:787–793. [PubMed: 16804544]
40. Irizarry RA, et al. The human colon cancer methylome shows similar hypo- and hypermethylation at conserved tissue-specific CpG island shores. Nat. Genet. 2009; 41:178–186. [PubMed: 19151715]
41. De Carvalho DD, et al. DNA methylation screening identifies driver epigenetic events of cancer cell survival. Cancer Cell. 2012; 21:655–667. [PubMed: 22624715]
42. Shimi T, et al. The role of nuclear lamin B1 in cell proliferation and senescence. Genes Dev. 2011; 25:2579–2593. [PubMed: 22155925]
43. Unterberger A, Andrews SD, Weaver IC, Szyf M. DNA methyltransferase 1 knockdown activates a replication stress checkpoint. Mol. Cell Biol. 2006; 26:7575–7586. [PubMed: 17015478]
44. Suzuki H, et al. Epigenetic inactivation of SFRP genes allows constitutive WNT signalling in colorectal cancer. Nat. Genet. 2004; 36:417–422. [PubMed: 15034581]
45. Zhang W, et al. Comparison of global DNA methylation profiles in replicative versus premature senescence. Life Sci. 2008; 83:475–480. [PubMed: 18723031]
46. Casillas MA Jr. Lopatina N, Andrews LG, Tollefsbol TO. Transcriptional control of the DNA methyltransferases is altered in ageing and neoplastically-transformed human fibroblasts. Mol. Cell Biochem. 2003; 252:33–43. [PubMed: 14577574]
47. Eden A, Gaudet F, Waghmare A, Jaenisch R. Chromosomal instability and tumours promoted by DNA hypomethylation. Science. 2003; 300:455. [PubMed: 12702868]

48. Gaudet F, et al. Induction of tumours in mice by genomic hypomethylation. Science. 2003; 300:489–492. [PubMed: 12702876]
49. Song JZ, Stirzaker C, Harrison J, Melki JR, Clark SJ. Hypermethylation trigger of the glutathione-S-transferase gene (GSTP1) in prostate cancer cells. Oncogene. 2002; 21:1048–1061. [PubMed: 11850822]
50. Landan G, et al. Epigenetic polymorphism and the stochastic formation of differentially methylated regions in normal and cancerous tissues. Nat. Genet. 2012; 44:1207–1214. [PubMed: 23064413]
51. O'Hagan HM, Mohammad HP, Baylin SB. Double strand breaks can initiate gene silencing and SIRT1-dependent onset of DNA methylation in an exogenous promoter CpG island. PLoS Genet. 2008; 4:e1000155. [PubMed: 18704159]
52. Ibrahim AE, et al. Sequential DNA methylation changes are associated with DNMT3B overexpression in colorectal neoplastic progression. Gut. 2011; 60:499–508. [PubMed: 21068132]
53. Nosho K, et al. DNMT3B expression might contribute to CpG island methylator phenotype in colorectal cancer. Clin. Cancer Res. 2009; 15:3663–3671. [PubMed: 19470733]
54. Carragher LA, et al. V600EBraf induces gastrointestinal crypt senescence and promotes tumour progression through enhanced CpG methylation of p16INK4a. EMBO Mol. Med. 2010; 2:458–471. [PubMed: 20941790]
55. Walsh CP, Chaillet JR, Bestor TH. Transcription of IAP endogenous retro-viruses is constrained by cytosine methylation. Nat. Genet. 1998; 20:116–117. [PubMed: 9771701]
56. O'Neill RJ, O'Neill MJ, Graves JA. Undermethylation associated with retroelement activation and chromosome remodelling in an interspecific mammalian hybrid. Nature. 1998; 393:68–72. [PubMed: 9590690]
57. Lee E, et al. Landscape of somatic retrotransposition in human cancers. Science. 2012; 337:967–971. [PubMed: 22745252]
58. De Cecco M, et al. Genomes of replicatively senescent cells undergo global epigenetic changes leading to gene silencing and activation of transposable elements. Aging Cell. 2013; 12:247–256. [PubMed: 23360310]
59. Dimri GP, et al. A biomarker that identifies senescent human cells in culture and in ageing skin *in vivo* . Proc. Natl Acad. Sci. USA. 1995; 92:9363–9367. [PubMed: 7568133]
60. Herbig U, Ferreira M, Condel L, Carey D, Sedivy JM. Cellular senescence in ageing primates. Science. 2006; 311:1257. [PubMed: 16456035]
61. Sedelnikova OA, et al. Senescing human cells and ageing mice accumulate DNA lesions with unrepairable double-strand breaks. Nat. Cell Biol. 2004; 6:168–170. [PubMed: 14755273]
62. Feinberg AP, Ohlsson R, Henikoff S. The epigenetic progenitor origin of human cancer. Nat. Rev. Genet. 2006; 7:21–33. [PubMed: 16369569]
63. Vredeveld LC, et al. Abrogation of BRAFV600E–induced senescence by PI3K pathway activation contributes to melanomagenesis. Genes. Dev. 2012; 26:1055–1069. [PubMed: 22549727]
64. Kennedy AL, et al. Activation of the PIK3CA/AKT pathway suppresses senescence induced by an activated RAS oncogene to promote tumorigenesis. Mol. Cell. 2011; 42:36–49. [PubMed: 21474066]
65. Pchelintsev NA, et al. the HIRA histone chaperone complex in the chromatin landscape. Cell Rep. 2013; 3:1012–1019. [PubMed: 23602572]
66. Debacq-Chainiaux F, Erusalimsky JD, Campisi J, Toussaint O. Protocols to detect senescence-associated beta-galactosidase (SA-betagal) activity, a biomarker of senescent cells in culture and in vivo. Nat. Protoc. 2009; 4:1798–1806. [PubMed: 20010931]
67. Harlow, E.; Lane, D. Antibodies: A Laboratory Manual. Cold Spring Harbor Laboratory Press; 1988.
68. Langmead B, Trapnell C, Pop M, Salzberg SL. Ultrafast and memory-efficient alignment of short DNA sequences to the human genome. Genome Biol. 2009; 10:R25. [PubMed: 19261174]
69. Krueger F, Andrews SR. Bismark: a flexible aligner and methylation caller for Bisulfite-Seq applications. Bioinformatics. 2011; 27:1571–1572. [PubMed: 21493656]
70. Hansen KD, Langmead B, Irizarry RA. BSmooth: from whole genome bisulfite sequencing reads to differentially methylated regions. Genome Biol. 2012; 13:R83. [PubMed: 23034175]

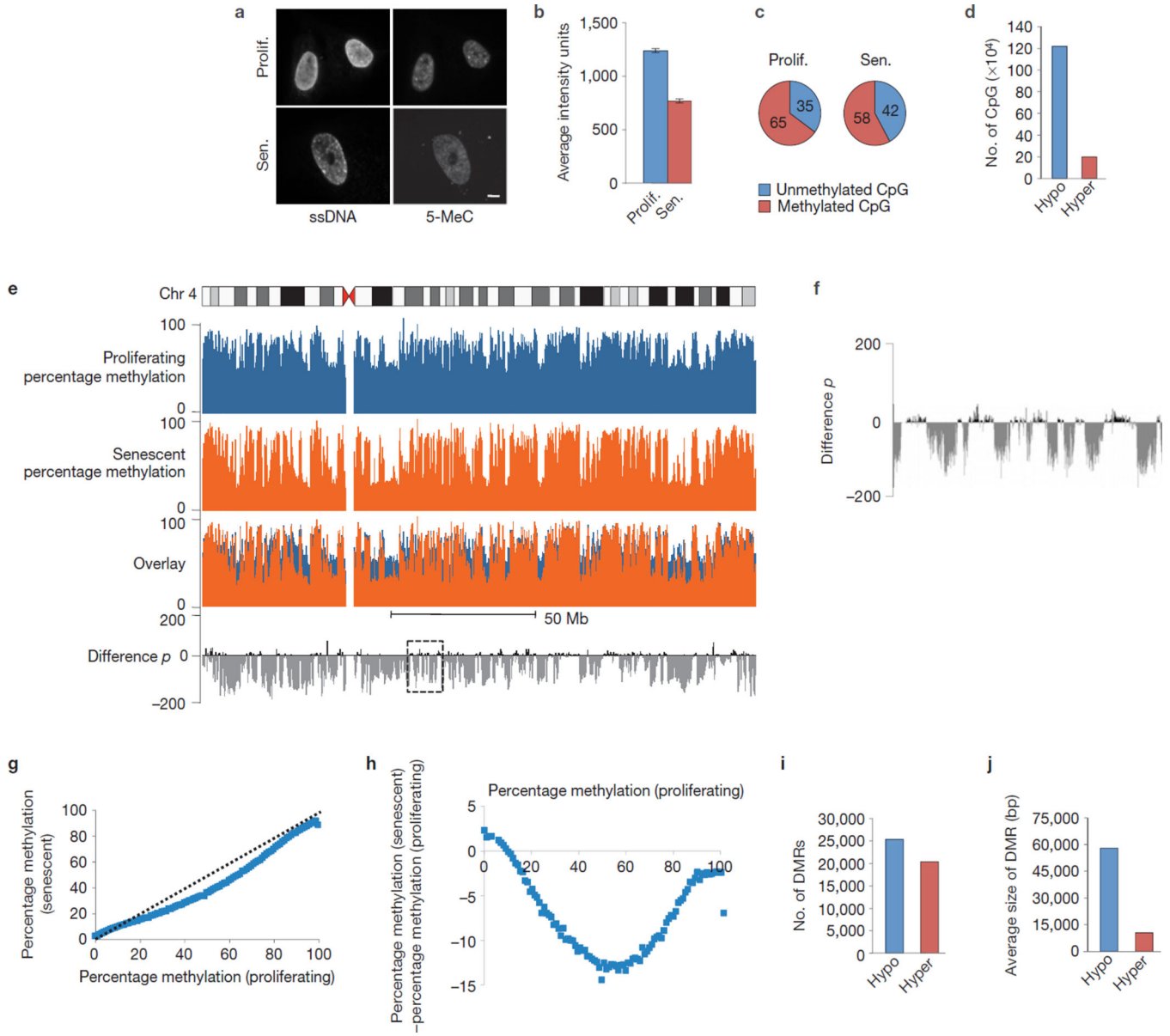


**Figure 1.**

Senescent cells exhibit overall hypomethylation and focal hypermethylation. (**a**) Proliferating (Prolif.) and senescent (Sen.) IMR90 cells stained for 5-methylcytosine (5-MeC) and single-stranded DNA(ssDNA). Scale bar, 5μm. (**b**) Quantitation of **a** in three independent experiments (100 cells each); error bars, mean ± s.e.m. (**c**) Percentages of methylated and unmethylated basecalls at reference CpG dinucleotides in proliferating and senescent cells. (**d**) Numbers of CpG dinucleotides becoming hypomethylated (hypo) and hypermethylated (hyper) in senescence. (**e**) Plot of chromosome 4 (chr 4) percentage methylation for proliferating and senescent cells. An overlay of these two plots is shown with difference *p*, proportional to the *P* value differences between methylation of proliferating and senescent cells. Negative and positive values are hypomethylation and hypermethylation, respectively. (**f**) Enlargement of boxed region from **e**. (**g,h**) Across the

whole genome, regions of intermediate methylation in proliferating cells tend to be hypomethylated in senescence. For **g** and **h** CpGs were split into 100 bins on the basis of proliferating methylation. The average senescent methylation/methylation difference of each bin was then computed and plotted. (**i**) Number of hypomethylated and hypermethylated DMRs (differentially methylated regions) over whole genome in senescent cells. (**j**) Average size of hypomethylated and hypermethylated DMRs over whole genome. bp, base pairs. For **c–j** data are from whole-genome bisulfite sequencing of three independent replicates.

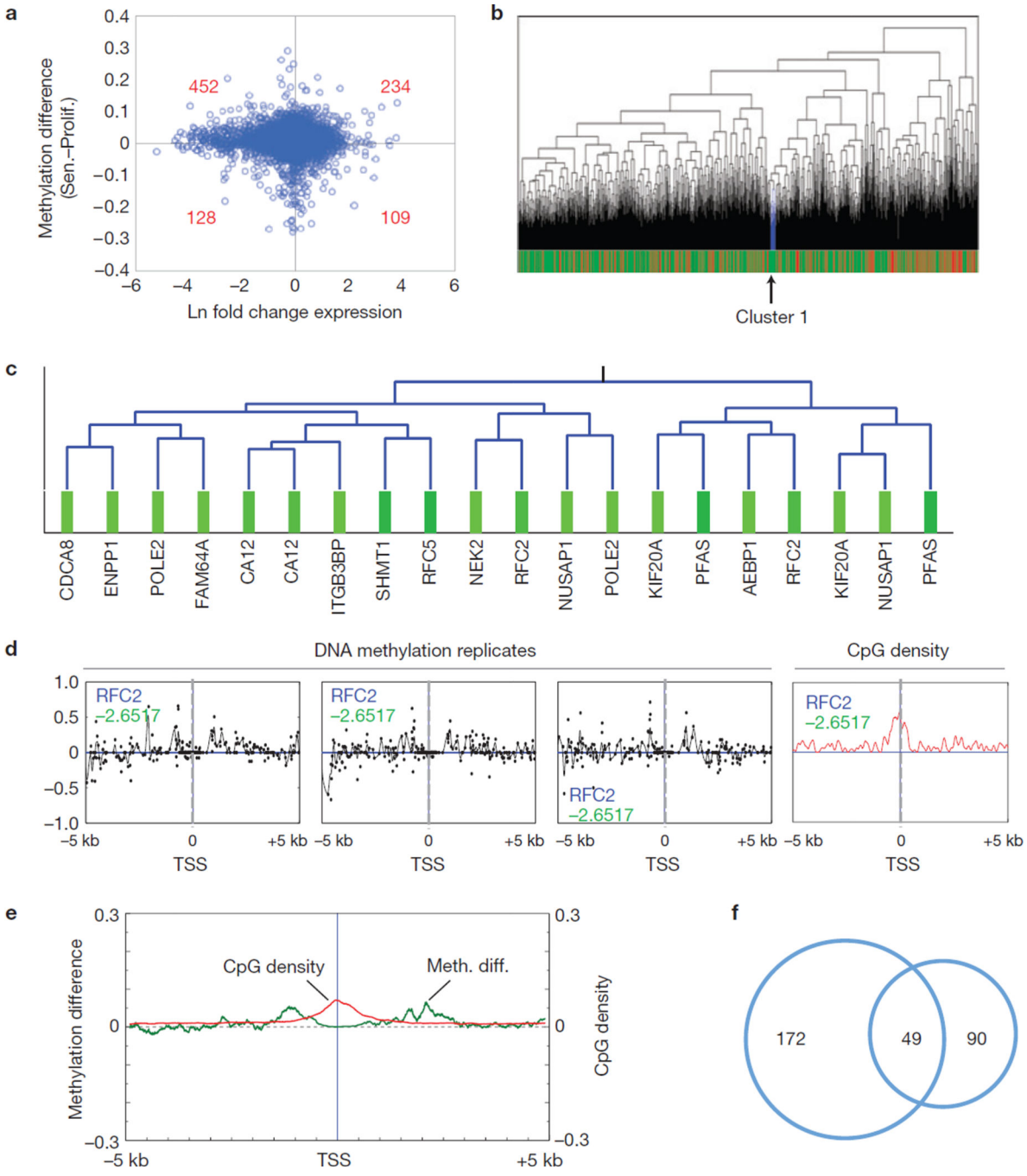


**Figure 2.**

Promoter proximal methylation of transcriptionally repressed cell cycle genes. (**a**) Ln fold change of gene expression between proliferating and senescent cells (positive values, increased expression in senescence; negative values, decreased expression in senescence) against the difference in promoter methylation between proliferating and senescent cells (Sen. - Prolif.). Analysis only for genes expressed above the median level of expression in proliferating cells. The red numbers show the number of genes (expressed in proliferating cells) with indicated directions of expression (FDR<0.05 and fold change >1.5) and

promoter methylation (FDR < 0.05) changes. (**b,c**). Example of a cluster (cluster 1) of downregulated genes with similar differential methylation signatures identified during execution of the gene list tool in ref. 23. (**b**) Cluster 1 location in a dendrogram of signatures arranged by shape. Green bars denote downregulated genes; red bars denote upregulated genes. Cluster 1 highlighted in blue and with arrow. (**c**) A close-up view of cluster 1, with gene names. Cluster 1 contains two replicates of the *RFC2* gene. (**d**) Three plots on the left: differential methylation versus position up- and downstream of the transcription start site (TSS) (−5kb (kilobases) to +5kb) of *RFC2* gene. The *y* axis is a differential methylation score that ranges from −1 to 1, denoting complete hypomethylation and hypermethylation, respectively. The vertical dashed centre line marks the TSS. Fold change (log2) gene expression is indicated in green. Data from all three replicates are shown. Rightmost plot: relative CpG density around *RFC2* gene TSS, plotted in red. (**e**) Average plot of differential methylation (green) versus position up- and downstream of TSS (−5kb to +5kb) for all 136 downregulated genes in Supplementary Table 11 (three upregulated genes are excluded), smoothed over 100 bp sliding windows. The left axis is average methylation difference, plotted in green. Units are in differential methylation (ranging from −1 to 1, as for **a**). The right axis is CpG density, plotted in red. Units are CpG sites per base pair. (**f**) Venn diagram showing overlap of genes in Supplementary Tables 9 and 11. Overlap = 27.0-fold enrichment over random, $P$ <0.0001.

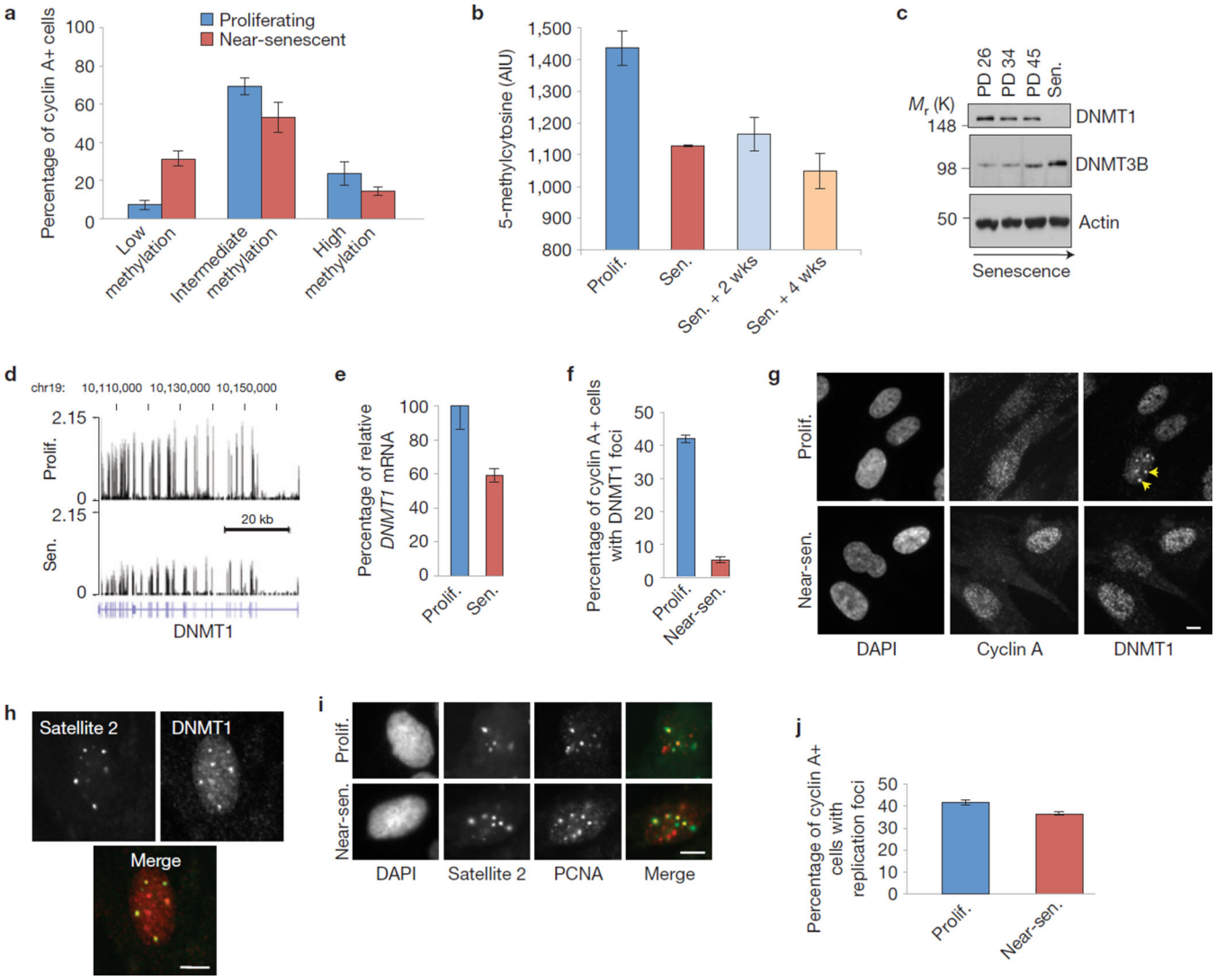


**Figure 3.**

DNA hypomethylation occurs before cell cycle exit and is associated with mislocalization of DNMT1. (**a**) Quantitation of 5-methylcytosine by immunofluorescence in cyclin-A-positive (cyclin A+) proliferating and near-senescent cells. See Supplementary Methods for definitions of Prolif, Near-sen and Sen. Low methylation denotes 900–1,700 average intensity units, intermediate methylation 1,800–2,200 units and high methylation 2,300–2,900 units. (**b**) Quantitation of 5-methylcytosine in proliferating (Prolif.), senescent (Sen.) and cells fixed 2 weeks and 4 weeks after onset of senescence, Sen.+2 wks and Sen.+4 wks respectively. (**c**) Western blot of DNMT1, DNMT3B and actin across indicated cell population doublings (PDs) and senescent cells. $M_r$ (K), relative molecular mass (thousands). (**d**) RNA sequencing (RNA-seq) analysis showing aligned reads (fragments per bp per million mapped reads) on *DNMT1* gene in proliferating and senescent cells. (**e**) Quantitative RT-PCR analysis of *DNMT1* expression in proliferating and senescent cells normalized to expression of *GAPDH* as a housekeeping gene. mRNA, messenger RNA. (**f**) Quantitation of proliferating and near-senescent cyclin A-positive cells containing DNMT1

foci (from **g**). (**g**) Immunofluorescence of DNMT1 and cyclin A in proliferating (Prolif) and near-senescent (Near-sen.) cells. Arrowheads mark DNMT1 puncta. DAPI, 4,6-diamidino-2-phenylindole. Scale bar, 5 μm. (**h**) Immuno-FISH of satellite 2 and DNMT1 with merge: DNMT1, red; satellite 2, green. Scale bar, 5μm. (**i**) Immunofluorescence *in situ* hybridization (immuno-FISH) of satellite 2, PCNA and merge: PCNA, red; satellite 2, green. Scale bar, 5 μm. (**j**) Quantitation of proliferating and senescent cyclin A-positive cells that contain PCNA foci. Source data for **a,b,e,f,j** in Supplementary Table 22. Uncropped images of blots/gels are shown in Supplementary Fig. 8e.

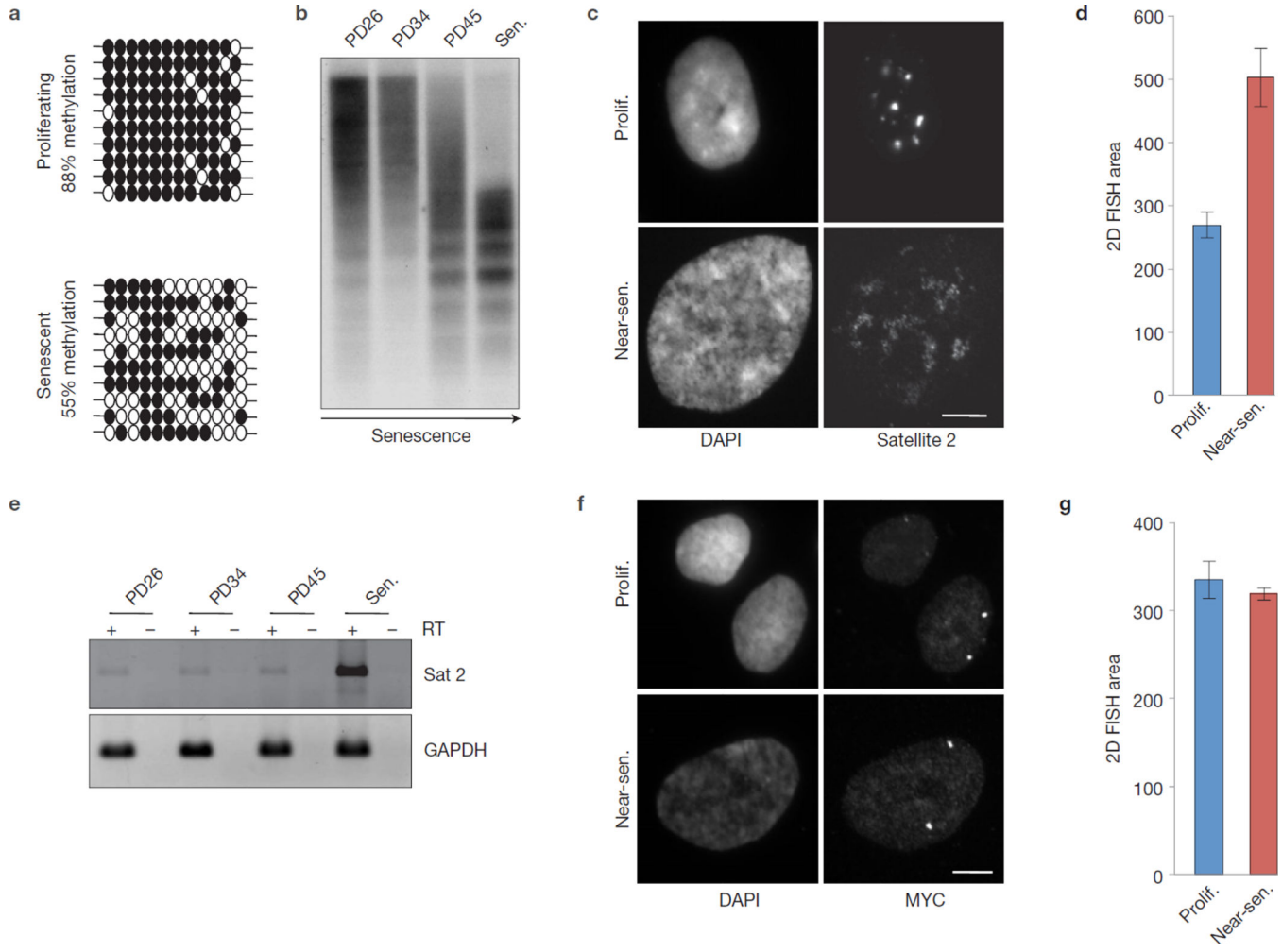


**Figure 4.**

Hypomethylation and expression of late-replicating satellite sequences in senescent cells. (**a**) Bisulfite sequencing of satellite 2 in proliferating and senescent cells. Each row represents an individual clone. Filled and open circles are methylated CpG and unmethylated CpG dinucleotides respectively. (**b**) Southern blot of genomic DNA with the methyl-sensitive enzyme BstBI probed with a probe specific for satellite 2. Genomic DNA was harvested at different timepoints as cells approach senescence as indicated by arrow. (**c**) FISH using a probe for satellite 2 in proliferating and near-senescent cells. Scale bar, 5μm. (**d**) Measurement of two-dimensional (2D) area occupied by the FISH probe from **c**. (**e**) RT-PCR of satellite 2 in IMR90 cells at indicated PD and senescence. (**f**) FISH using a probe for *MYC* in proliferating and near-senescent cells as a negative control for **c**. Scale bar, 5μm. (**g**) Measurement of the two-dimensional area occupied by the *MYC* FISH probe in **f**. For all graphs, error bars indicate the mean ± s.e.m. of three independent experiments where 100 cells were scored per experiment. Source data for **d,g** in Supplementary Table 22.

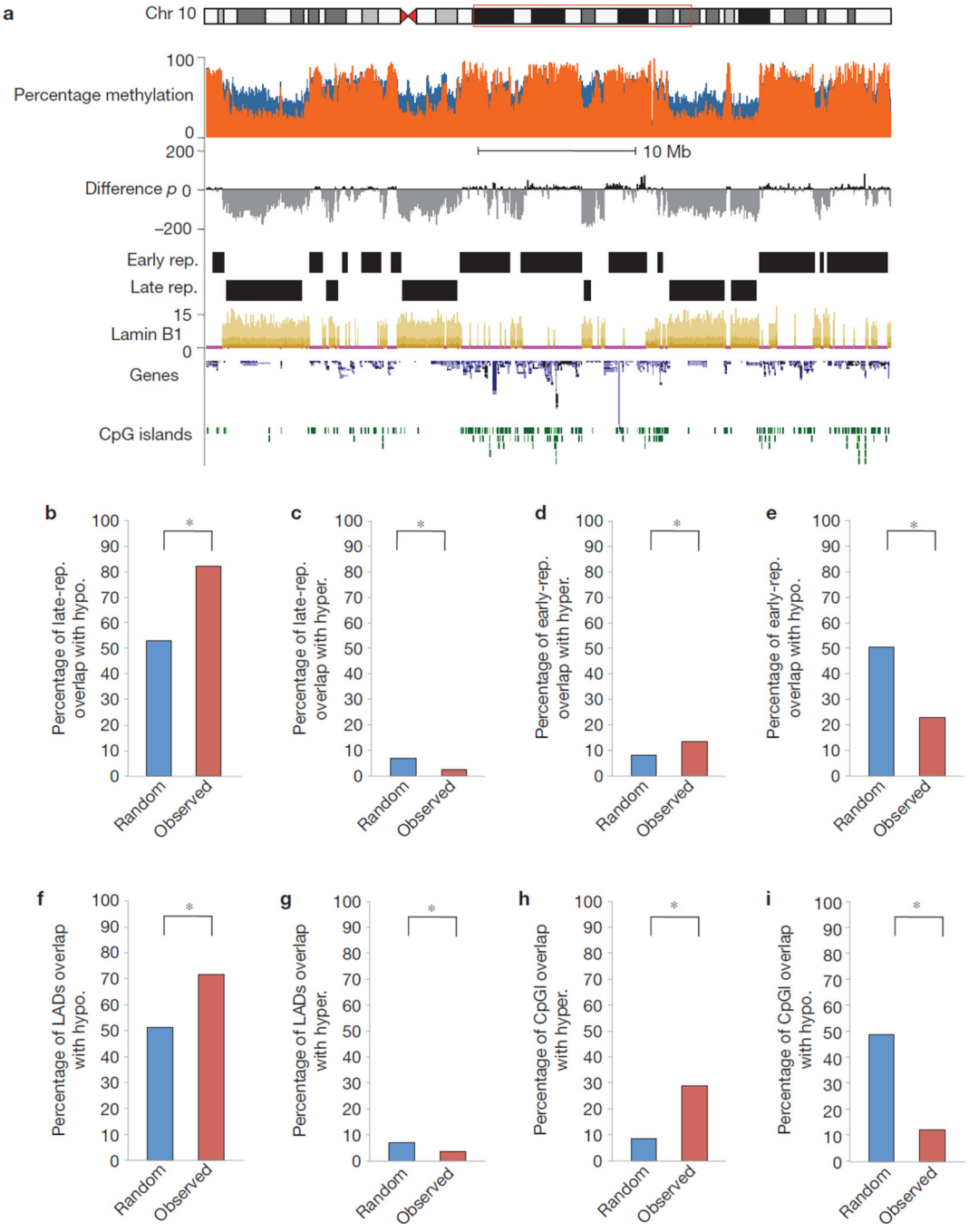


**Figure 5.**

Hypomethylation occurs at gene-poor, late-replicating and lamin-associated domains whereas hypermethylation occurs at gene-rich, early-replicating regions and CpG islands. (**a**) Plot of a 43.5 Mb (megabase) region of chromosome 10 (chr 10) percentage methylation of proliferating (blue) and senescent (orange) cells with difference *P* (Fig. 1e). Normalized enrichment of lamin B1 determined by chromatin immunoprecipitation sequencing of proliferating IMR90 cells is shown. Early- and late-replicating sequences from[31] are annotated. Genes and CpG islands are from UCSC. (**b–i**) Plots showing percentage overlap

in total base pairs of indicated features across the whole genome, comparing observed and random predicted values. Asterisks indicate statistical significance and $P < 0.001$.

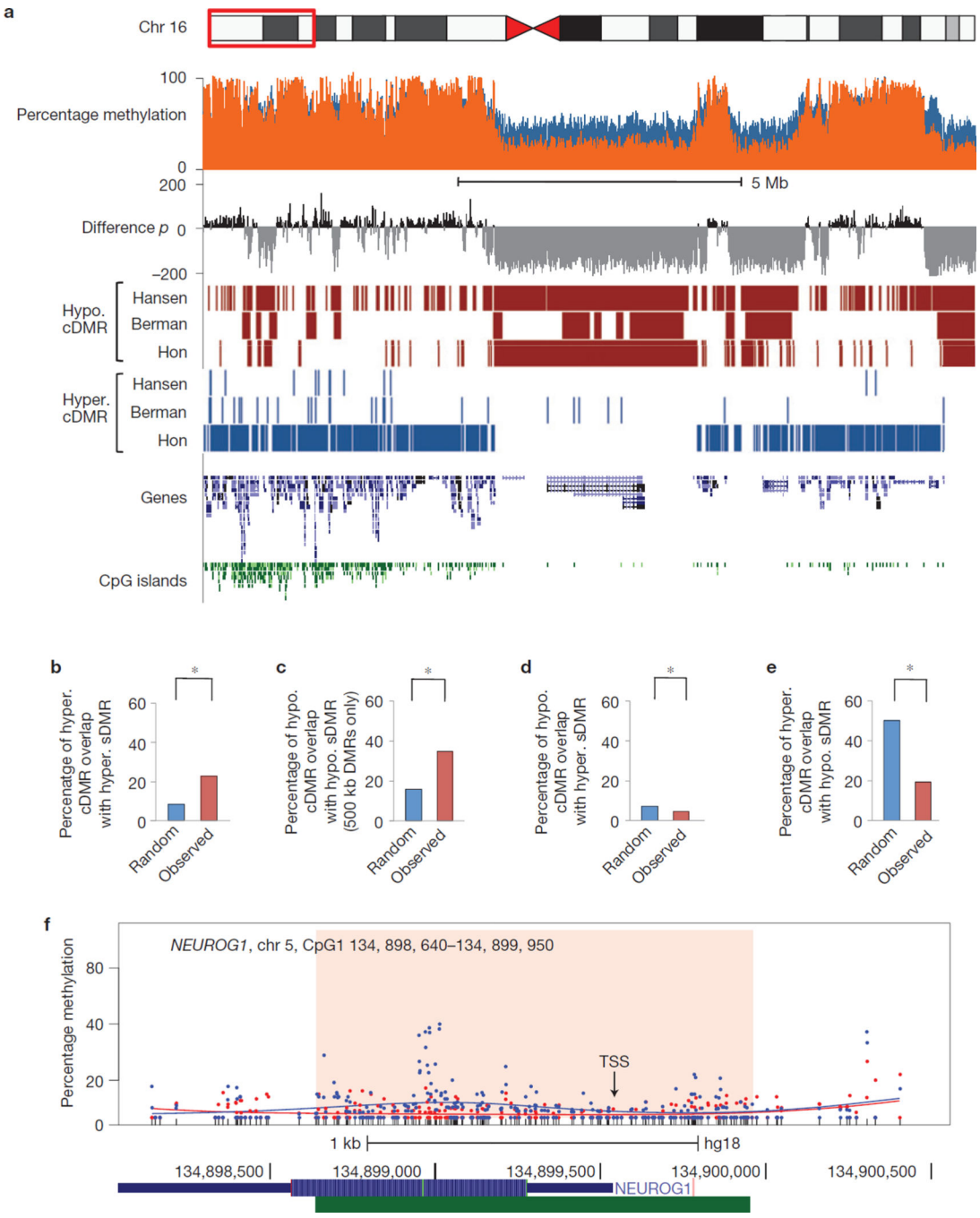


**Figure 6.**

Methylation changes in senescence resemble those in cancer. (**a**) Plot of a 13.5 Mb region of chromosome 16 (chr 16) with percentage methylation in proliferating (blue) and senescent (orange) cells and difference *p* (Fig. 1e). Genes and CpG islands are shown. Hypomethylated and hypermethylated DMRs from colon and breast cancer, hypo. cDMR and hyper. cDMR respectively, are mapped from[3,35,36]. (**b–e**) Plots of percentage overlap in total base pairs of indicated features across whole genome, comparing observed and random predicted values; cDMRs taken from ref. 36. Asterisks indicate statistical significance and

*P*-value $\ll$ 0.001. (**f**) Increased methylation of neurogenin 1 (*NEUROG1*) CpG island in senescence. Plot of percentage methylated basecalls in proliferating (orange) and senescent cells (blue), at the *NEUROG1* gene, from whole-genome bisulfite sequencing data of three replicates of proliferating cells and three replicates of senescent cells. The orange and blue lines show the smoothed average percentage methylated basecalls at corresponding CpGs. Individual CpGs are indicated by black ticks along the *x* axis. The UCSC *NEUROG1* gene (blue bar (hatched, exon 1)) and CpG island (green bar) are also shown. The TSS is indicated by a vertical black arrow. The gene, chromosome and bp of the CpG island are indicated at the top left.

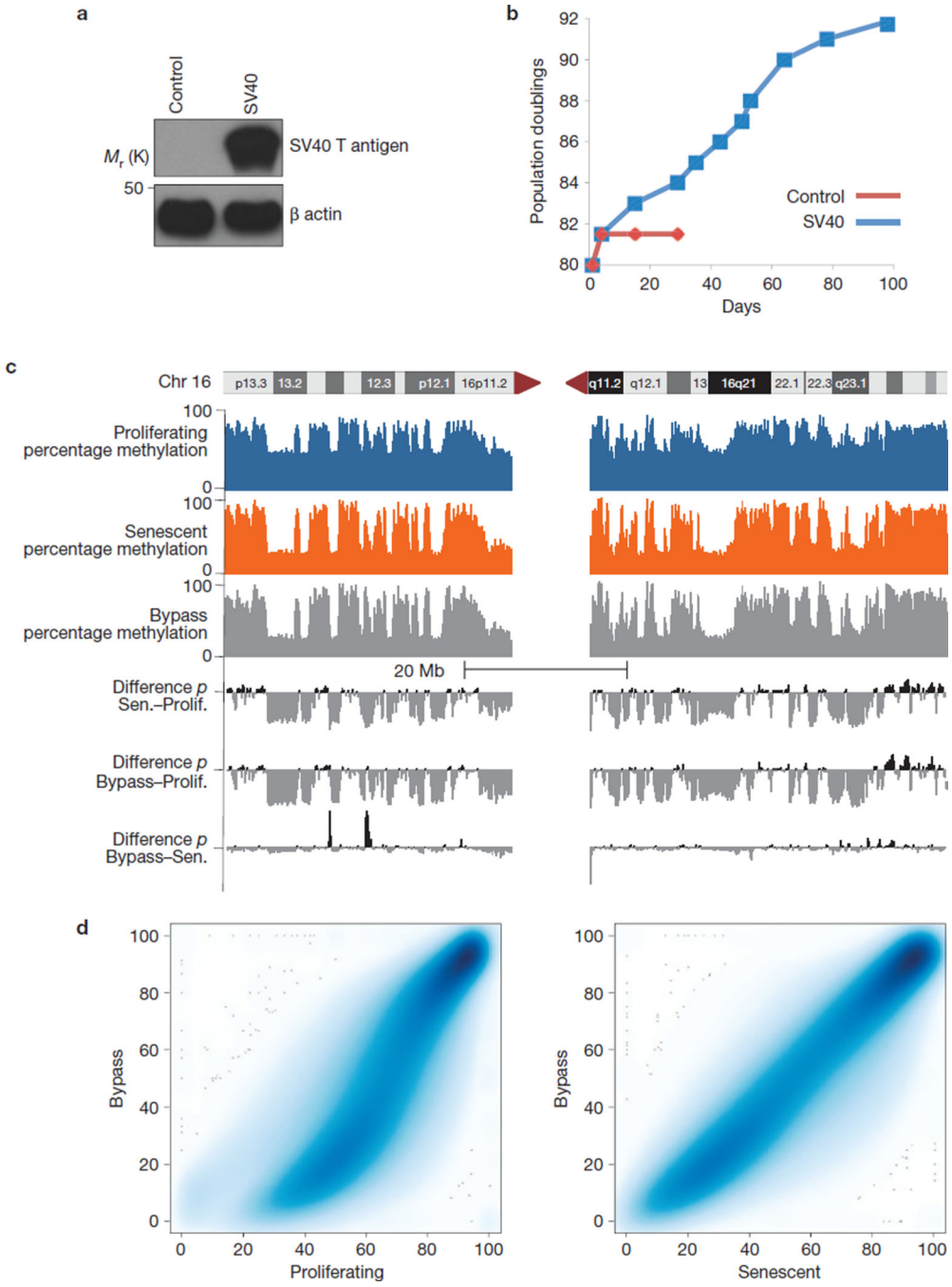


**Figure 7.**

Altered methylation is retained in cells that bypass senescence. (**a**) Three replicates of IMR90 cells approaching senescence (PD 80; Supplementary Fig. 1a) were infected with a control lentivirus or a lentivirus encoding SV40 T antigen. $M_r$ (K), relative molecular mass (thousands). (**b**) SV40 T antigen-expressing cells exhibit extension of lifespan (bypass). (**c**) DNA was collected for whole-genome bisulfite sequencing from bypass cells at PD 84. Plot of chromosome 16 (chr 16) with percentage methylation for proliferating, senescent and bypass Senescent cells. Difference *P* is proportional to the *p* value difference between

methylation of proliferating and senescent cells (difference *P*, Sen. -Prolif.), proliferating and bypass cells (difference *P*, Bypass - Prolif.) and senescent versus bypass cells (difference *P*, Bypass - Sen.). Negative and positive values are hypomethylation and hypermethylation respectively. (**d**) Plot of percentage methylation in 2kb windows encompassing whole genome, comparing either bypass against proliferating cells (left) or bypass against senescent cells (right).

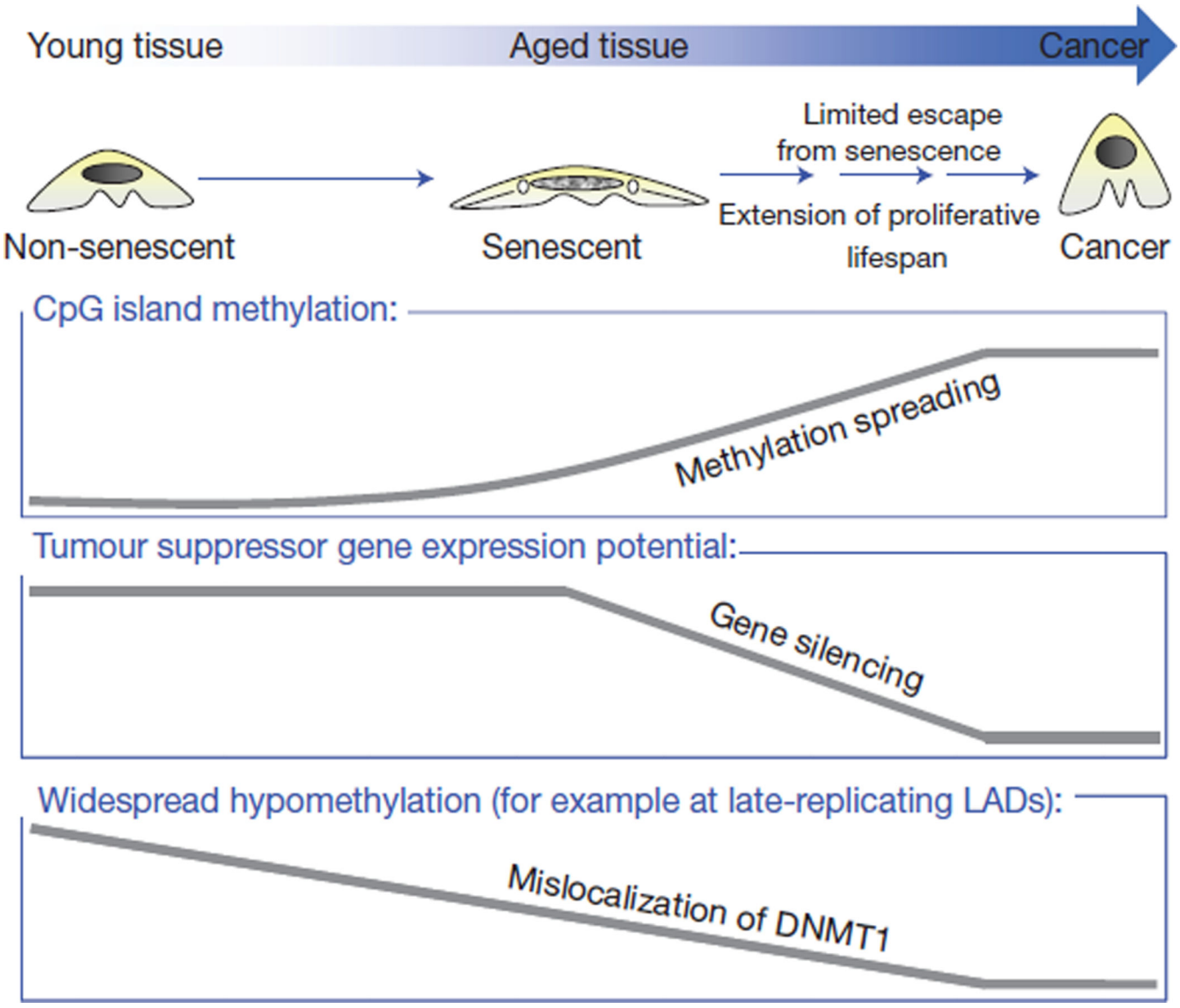


**Figure 8.**

The altered epigenome of senescent cells might promote age-associated increase in incidence of human cancers. Our analyses and previous studies and ideas[62] lead to the following model. Senescent cells accumulate with age in human tissues[59]. These senescent cells harbour low-level methylation of CpG islands of tumour suppressor genes that is insufficient to silence gene expression. However, even a limited/transient escape from senescence, for example owing to genetic inactivation of PTEN[63,64], confers further rounds of cell division that permits proliferation-dependent spreading of DNA methylation[51]. Hence, an initial 'seed' of methylation in a senescent cell in an aged tissue can, in conjunction with other genetic alterations and clonal selection, grow to full CpG island hypermethylation and tumour suppressor gene silencing, thereby facilitating progression to late-life cancer. Global hypomethylation in senescent cells may also promote genome instability and dysfunction[3,47,48,55–58]